



Surface Porous Microstructured Fibers with Customized Functionalities for 1D Functional Materials

Junxian Huang, Xiaoyang Guan, Bingang Xu, Jianliang Gong, Yuanyuan Gao, Meiqi Li*

† Nanotechnology Center, Institute of Textiles and Clothing, The Hong Kong Polytechnic
University, Hung Hom, Kowloon, Hong Kong, P.R. China

* Corresponding Author. E-mail: tcxubg@polyu.edu.hk; Tel: +852-2766 4544

ABSTRACT: Fibers have been widely used for wearable textiles and fiber-reinforced composites owing to their unique structures and performances. However, design and fabrication of 1D advanced fiber materials with diversified surface microstructures and desired functionalities is still a considerable challenge. In this study, we present a novel one-dimensional confined breath figure (1D-cBF) approach for efficient preparation of a brand-new kind of 1D continuous fibers surface-engineered with conformal honeycomb porous microstructures (F@HPMs) and a novel kind of Hybrid F@HPMs (HF@HPMs) with functional nanomaterials incorporated in porous microstructures. The obtained F@HPMs demonstrated controllable surface microstructural morphologies by adjusting the experimental variables, and the main influential factors including solvents, concentrations, polymer bricks, and substrates in the 1D-cBF process were systematically studied. Moreover, various functional nanocomponents could be incorporated for developing HF@HPMs for customized functionalities. As a demonstration, TiO₂/HF@HPMs that incorporate with TiO₂ nanoparticles were fabricated for enhanced photodegradation of organic pollutants.

Keywords: conformal porous structure; composite; fiber material; photocatalytic degradation

1. Introduction

Wearable textiles are a kind of lightweight, flexible, and wearable materials fabricated from natural or synthetic fibers. In terms of dimension, filament and staple fiber are categorized as

one-dimensional (1D) materials that are the smallest visible unit of wearable textiles. 1D staple fiber or filament can be obtained by various spinning methods, such as wet spinning, dry spinning, melt spinning, and electrospinning. By utilizing various methods like twisting, twining or blending, these materials can be formed into continuous multifilament fibers.^{1,2} 1D continuous fibers are not only the most fundamental materials of wearable textiles but also can be developed into 1D advanced functional materials for various advanced applications in communicating,³ actuating,⁴ sensing,⁵ illuminating,⁶ energy harvesting,⁷ and drug delivery.⁸ Owing to their inherent flexibility, such kind of 1D advanced functional fibers can be further processed with stitching, sewing, knitting or weaving into 2D or 3D functional fabrics for a broad range of novel applications in wearable technology, smart home, and healthcare.⁹⁻¹³

In practical applications, 1D continuous fibers and textile materials often require further modification to endow them with unique features or desirable functionalities. Conventional methods towards the modification of textile/fiber materials involve physical methods (e.g., coating, spraying, physical vapor deposition, and laminating.¹⁴⁻¹⁷) and chemical methods (e.g., plasma treatment, electrochemical deposition, in situ synthesis, graft modification, and cross-linking.¹⁸⁻²³). Besides, the usage of “self-seeding” strategy can also prepare the uniform 1D-fiber with controlled length and nanostructures.^{24,25} Although great progress has been achieved in the design and fabrication of 1D advanced fiber materials, there remain challenges in endowing the fiber substrates with desired functions or structures meanwhile maintaining their inherent surface texture and properties. For example, traditional coating methods will introduce

a solid layer on fiber materials' surface, resulting in adverse effects on their intrinsic advantages (e.g., flexibility, air permeability) and making them no longer suitable for loading functional additives that require high exposing area. Porous microstructure, however, can effectively improve a material's physicochemical properties owing to the increased specific surface area.^{26,27} Therefore, introducing functional nanocomponents into a fiber with conformal porous microstructures would be an effective and attractive approach for combining the advantages of the strategies stated above.

Breath Figure (BF) refers to the phenomenon in which water vapor condensation on the cold substrate follows by forming mist water droplets.^{28,29} This process was usually utilized as a green and versatile soft-template method for the construction of honeycomb porous films (HPFs) with controlled porous microstructures and surface properties.³⁰⁻³² More recently, our group reported a new strategy to fabricate conformal porous microstructured 2D fabrics by the BF process.³³⁻³⁵ The obtained fabrics showed improved mechanical and thermal insulation properties, and meanwhile maintained the excellent intrinsic properties of the original fabrics like flexibility, air permeability, etc. Considering its low cost, economical, and nondestructive characteristics, the BF process is expected to be an ideal approach in the fabrication and modification of fiber materials. While modifying 2D fabrics with refined structures to introduce desired functions presents a promising application prospect, directly developing 1D fiber materials with elaborate microstructure and customized functionalities can bring even more encouraging and creative benefits owing to the larger specific surface area and length-diameter

ratio as compared with their 2D equivalents. However, the formation of conformal honeycomb porous microstructures (HPMs) on 1D fiber substrates is more challenging than that on 2D planar substrates. The conventional drop cast or spin coating method are no longer suitable for introducing polymer solution during the 1D confined breath figure (1D-cBF) process because the solution cannot uniformly cover the whole surface of a “cylindrical” fiber. Besides, some multifilament fibers have loose and uneven surface morphology, making it more difficult to form ordered porous microstructures contouring to the nonplanar fiber surface. A survey of the literature has shown that no systematic study is conducted or reported in this area. To this end, developing 1D-cBF approach for the design and fabrication of a new kind of 1D fiber materials is essential for practical applications and inspiring new attention to the material design and functions innovation of fiber materials.

Herein, a novel 1D-cBF approach with the characteristics of easily scalable, nondestructive was developed for simple, economical and efficient fabrication of a brand-new kind of 1D continuous fibers surface-engineered with conformable honeycomb porous microstructures (F@HPMs). The main influential factors in the 1D-cBF process including solvents, concentrations, polymer bricks, and fiber substrates, and their influence on the formation of surface porous microstructures were systematically studied. The obtained F@HPMs demonstrated customizable and controllable microstructure morphologies by adjusting the experimental variables. Furthermore, this new 1D-cBF technique can also be used for straightforwardly manufacturing a new kind of Hybrid F@HPMs (HF@HPMs) that incorporate

desired functional nanomaterials in the porous microstructures. By elaborately controlling the surface porous microstructures, the resultant HF@HPMs shows a larger specific surface area and excellent capacity to load the functional nanomaterials with an alleviative embedded phenomenon. As a demonstration of application, the TiO₂/HF@HPMs that incorporated with photocatalytic active TiO₂ nanoparticles were fabricated for the photodegradation of organic pollutants, and the TiO₂/HF@HPMs showed enhanced performance on photocatalytic degradation of pollutants as compared with control samples. These performance-enhanced HF@HPMs can take better advantages of the loaded nanomaterials and possess the customized multifunction of the introduced components, which is expected to broadly extend the application fields of 1D fiber materials to meet specific advanced requirements.

2. Materials and Methods

2.1. Materials

Polystyrene-*block*-Polybutadiene-*block*-Polystyrene (SBS, M_w ~133800), Poly (dimethylsiloxane)-*graft*-Polyacrylates (PDMS-*g*-PAs, M_n ~26000, dimethylsiloxane composite: ~80 wt%), Poly (methacrylic acid methyl ester) (PMMA, M_w ~120000), Chloroform (CHCl₃, anhydrous, ≥99.9%), Carbon disulfide (CS₂, anhydrous, ≥99.9%), Tetrahydrofuran (THF, ≥99.9%) were purchased from Sigma-Aldrich Co. Titanium Dioxide Nanoparticles (TiO₂ NPs), Copper Nanoparticles (Cu NPs), Zinc Oxide Nanowires (ZnO NWs), and Silver Nanowires (Ag NWs) were purchased from XFNANO, Inc. Methylene blue

trihydrate (MB, $\geq 82\%$) was purchased from Sinopharm Chemical Reagent Co., Ltd. All reagents were used as received without further purification. Silver-plated polyester (SPP) multifilament fibers and Steel multifilament fibers were bought from the 3M company. Poly (ethylene terephthalate) (PET) fibers were provided by a local textile company.

2.2. Preparation of F@HPMs via 1D-cBF Method

The fibers were first rinsed with a nonionic detergent aqueous solution and deionized (DI) water several times, followed by drying in an oven and kept in a desiccator. The polymer solution was prepared by dissolving different amounts of polymers (e.g., SBS, PDMS-g-PAs, PMMA) in the selected solvent (e.g., CHCl_3 , CS_2 , THF) with the concentration of 100 mg/ml, 150 mg/ml, 200 mg/ml, 250 mg/ml, respectively. For example, the SBS/ CHCl_3 solution with a concentration of 150 mg/ml was prepared by adding 3 g SBS into a bottle with 20 ml of CHCl_3 as the solvent, and after magnetic stirring at ambient temperature ($\sim 25^\circ\text{C}$) for 2 h, the transparent SBS/ CHCl_3 polymer solution was successfully prepared. The high-humidity environment was created by adding a small amount of DI water into a well-sealed wide-mouth bottle beforehand. In a typical 1D confined Breath Figure (1D-cBF) procedure, PET fiber, for example, was coated with the prepared polymer solution by dip-coating method, and then transferred to the sealed wide-mouth bottle immediately. The 1D-cBF process was conducted at ambient temperature for 15 min. Finally, the novel kind of fiber surface-engineered with honeycomb porous microstructures (F@HPMs) was obtained by spontaneously drying the

residual water on the fiber's surface for 30 min under an oven at 50°C, and then kept in a desiccator for further experiment and characterization.

2.3 Preparation of HF@HPMs via 1D-cBF Method

To study the feasibility and versatility of the 1D-cBF strategy to incorporate functional nano-additives with different kinds of fibers for the straightforward fabrication of Hybrid F@HPMs (HF@HPMs), various nanomaterials (e.g., TiO₂ NPs, Cu NPs, ZnO NWs, and Ag NWs, etc.) were blended into the SBS/CHCl₃ solution (150 mg/ml, additives/polymer was set at 1:20 in the mass ratio) to form the hybrid suspension. After ultrasonication and magnetic stirring for 30 min at ambient temperature (~ 25°C), the well-dispersed hybrid suspension was obtained. The HF@HPMs were directly fabricated with the hybrid solution by the same 1D-cBF process.

2.4 Photocatalytic Degradation of Organic Pollutant

Several silver-plated polyester (SPP) multifilament fibers were selected, tailored, and weighed. The length of each fiber was fixed at 3.5 cm and the total weight of these fibers was 0.056 g. Then, the SPP-based HF@HPMs that were incorporated with TiO₂ NPs *via* 1D-cBF approach (i.e., TiO₂/HF@HPMs) were fabricated, tied together, and put into a 5-mL bottle filled with methylene blue (MB) aqueous solution (1.65×10^{-5} M). The photocatalytic degradation process was conducted using a 365 nm UV light tube within a dark chamber, and the power of the light

was 18 W. The distance between the UV light and samples was set at 10 cm. As a control, another group of SPP multifilament fibers with the same size and weight were prepared and fabricated into TiO₂/HF@Solid coating by the conventional coating method. Furthermore, to better highlight the advantages of 1D functional fibers than the 2D fabrics, a well-tailored fabric (1 cm × 3.5 cm, 0.063 g) that was woven from the same SPP multifilament fibers was manufactured. The fabric was then modified with BF method to create surface porous microstructures loaded with TiO₂ NPs (i.e., TiO₂/Fabric@HPMs) for comparison. These two control samples were conducted with the same photocatalytic degradation process to compare their performance with TiO₂/HF@HPMs. The degradation efficiency was calculated by the following equation:

$$D_e = 100 \times (A_0 - A_t)/A_0 \quad (1)$$

where A_0 is the initial absorption intensity of MB at 664 nm, A_t is the absorption intensity of MB at 664 nm at different degradation times, and D_e is the degradation efficiency of MB (%).

2.5. Characterization

The surface microstructural morphologies of the F@HPMs and HF@HPMs prepared by different experimental parameters were obtained by scanning electron microscopy (SEM, TESCAN VEGA3) under 15.0 kV accelerating voltage after being coated with a thin layer of

sputtered gold (2 nm). The elemental analysis of HF@HPMs was analyzed using a SEM equipped with an Energy Dispersive Spectrometer (EDS). The photocatalytic activity of the prepared fibers/fabric was investigated using a digital camera and a UV-Visible absorption spectrometer (UV-Vis, Lambda 18) to monitor the photocatalytic degradation efficiency of organic pollutants with time, respectively. The mechanical property tests were carried using a universal tensile testing machine (Instron Co., Ltd.) at a loading rate of 5 mm/min. Each fiber sample was stabilized on a self-made frame with a gauge length of 3 cm, and the number of the tested samples were at least five.

3. Results and Discussion

3.1. Proposed 1D-cBF Strategy of F@HPMs and HF@HPMs

The preparation process of fibers surface-engineered with honeycomb porous microstructures (F@HPMs) and hybrid F@HPMs (HF@HPMs) *via* the 1D-cBF strategy is shown in Figure 1. Firstly, a fiber substrate was directly immersed into the polymer solution with the selected concentration and then transferred to a high-humidity environment immediately (Figure 1a,b). Through the evaporative cooling of the volatile solvent in the moisture environment, water nuclei would be introduced on the surface of the fiber by nucleation (Figure 1c,d). Then, the water nuclei would gradually grow and self-assemble into ordered water droplet arrays by the Marangoni convection effect (Figure 1e).³⁶ These water droplet arrays then served as soft templates for the formation of the honeycomb porous microstructure of polymers based on the

nonsolvent induction effect.³⁷ After subsequent drying in a low-humidity environment, the fiber with conformal surface porous microstructures was successfully obtained (Figure 1f). The HF@HPMs can be directly fabricated by changing the polymer solution into hybrid suspension composed of polymer solution and functional nanomaterials *via* the same 1D-cBF technique, as illustrated in Figure 1g-k. After evaporation of liquid residuals, the fiber with incorporation of functional nanomaterials in the conformal surface porous microstructures would be obtained (Figure 1k).

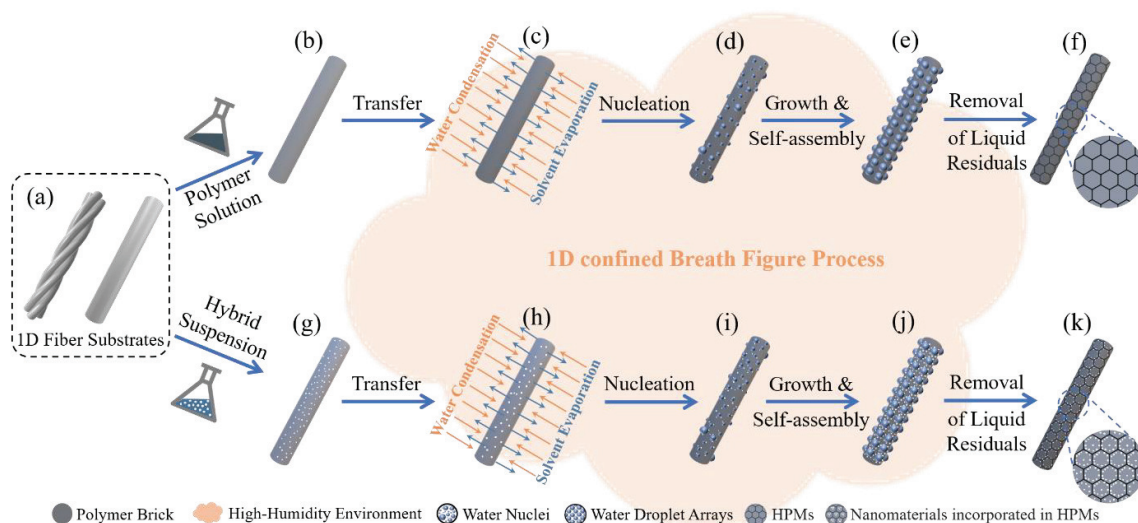


Figure 1. Schematic illustration of the preparation of the F@HPMs and HF@HPMs.

3.2. Influence of Solvent and Solution Concentration on the Formation of F@HPMs

The solvent used to dissolve polymer bricks was considered as one of the most important factors that affect the formation of F@HPMs. According to the mechanism of porous microstructures formation,^{38,39} solvents that have the characteristics of low boiling point and high immiscibility

with water are ideal candidates for the 1D-cBF process. Besides, the interfacial tension with water and the surface tension of the solvent are also significant factors that cloud affect the surface morphologies of the resultant F@HPMs. Table S1 shows three solvents used in this study and their physicochemical properties. The surface morphologies of PET-based F@HPMs prepared from SBS as polymer brick with different kinds of solvent at a concentration of 150 mg/ml are shown in Figure 2. First, we chose CHCl_3 , a wide-used solvent in the BF method, for the formation of F@HPMs *via* 1D-cBF approach. As demonstrated in Figure 2a-d, HPMS can successfully form on the PET fiber surface. When changing the solvent to CS_2 , similar porous microstructures can be found, as shown in Figure 2e-h. However, the average spacing distance of HPMS formed by CS_2 is about $0.29 \mu\text{m}$ (see inset of Figure 2h) which is much shorter than that form by CHCl_3 ($\sim 0.48 \mu\text{m}$, Figure 2d inset). This is possibly due to the CS_2 has a lower water solubility and higher interfacial tension with water than CHCl_3 (Table S1). Besides, the higher anisotropy of the pores formed by SBS/ CS_2 solution during the 1D-cBF process is mainly due to the high coalescence tendency between water droplets, which is considered as a crucial effect that hinders the formation of conformal porous microstructure.^{28,40} The relatively low viscosity of CS_2 solvent may have assisted the coalescence phenomenon. When choosing a water-miscible THF as the solvent, wrinkled structures instead of HPMS were observed on the surface of the PET fiber. In consideration of the formation mechanism of honeycomb porous microstructures, the evaporative cooling in a high-humidity environment of THF will result in the formation of water droplets on the solution. Once the droplets contact with the THF, these droplets cannot stabilize and maintain the shape as a sphere but will spread

out due to their high miscibility,⁴¹ thereby forming a wrinkled structure after the drying of both THF and water.

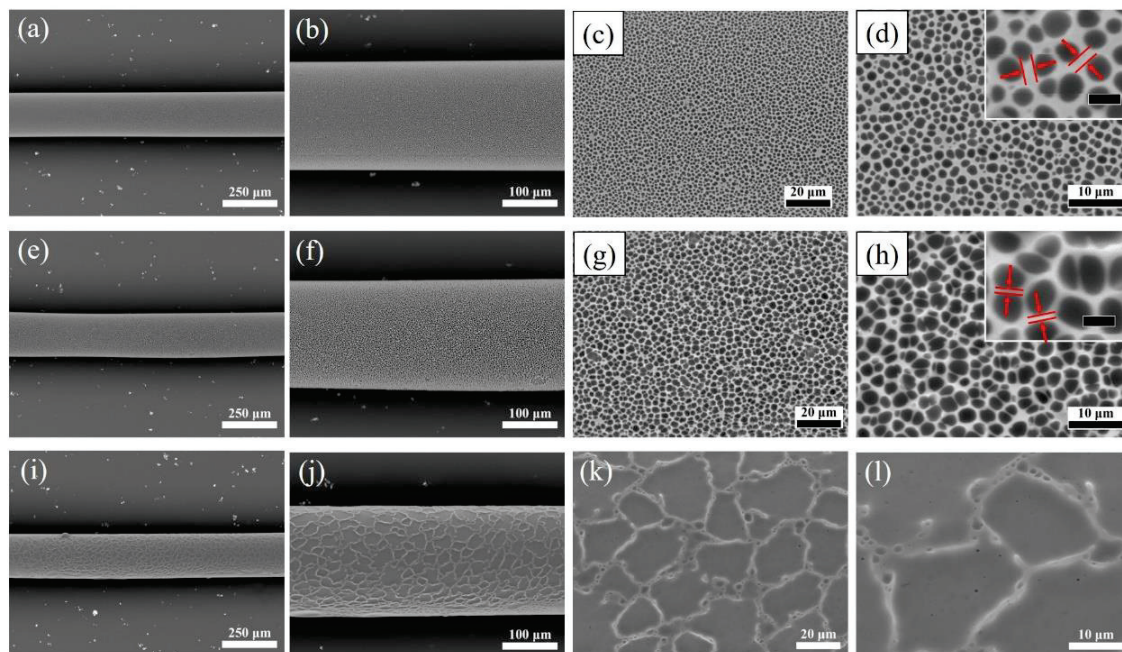


Figure 2. Typical SEM images of the PET-based F@HPMs prepared from SBS with different solvents at the concentration of 150 mg/ml *via* 1D-cBF approach: (a-d) CHCl₃, (e-h) CS₂, and (i-l) THF. The insets of (d) and (h) are their magnified views correspondingly (scale bar: 2 μm).

Solution concentration is another important factor that affects the formation of F@HPMs. To investigate the influence of solution concentration on the construction of F@HPMs, SBS and CHCl₃ were chosen as brick material and solvent, respectively. Figure 3a-a'' show the surface morphologies of pristine PET fiber at different magnifications. The surface of the pristine PET is very smooth without any porous microstructures even at high magnification (Figure 3a''). When conducting the 1D-cBF process with SBS/CHCl₃ at a relatively low solution concentration (100 mg/ml), only some irregular and disordered porous structures can be observed (Figure 3b-b''), indicating that a low concentration of the solution is not able to form

uniform HPMS. This phenomenon is possibly due to the following reasons: when using a polymer solution with insufficient concentration for the 1D-cBF process, the solution cannot uniformly cover the whole surface of a fiber, so the resultant porous microstructures are irregular. Besides, the viscosity of the polymer solution will decrease as the concentration decreases, and the polymer protective layers are not strong enough to stabilize water droplets, resulting in the heterogeneity of porous microstructures.⁴² The average size of these irregular porous structures is about 1.2 μm (Figure 3f). When increasing the solution concentration to 150 mg/ml, continuous and regular HPMS with the average pore size of 1.8 μm (Figure 3c-c'' and g) are beginning to form on the fiber surface. With the increase of solution concentration to 200 mg/ml, more narrowly dispersed pores were found on the fiber surface, as demonstrated in Figure 3d-d'', and the pore size becomes smaller (~ 1.3 μm , Figure 3h) as compare to their low concentration counterparts. When the concentration reaches 250 mg/ml (Figure 3e-e''), the average pore size further reduces to 0.92 μm (Figure 3i), and some uneven pit can be observed on the fiber surface at a middle magnification, as shown in Figure 3e', implying that the excessive solution concentration can hinder the formation of F@HPMS. To better illustrate the size of porous microstructure, the average pore sizes of PET-based F@HPMS prepared from SBS/ CHCl_3 with different concentrations are plotted in Figure S1.

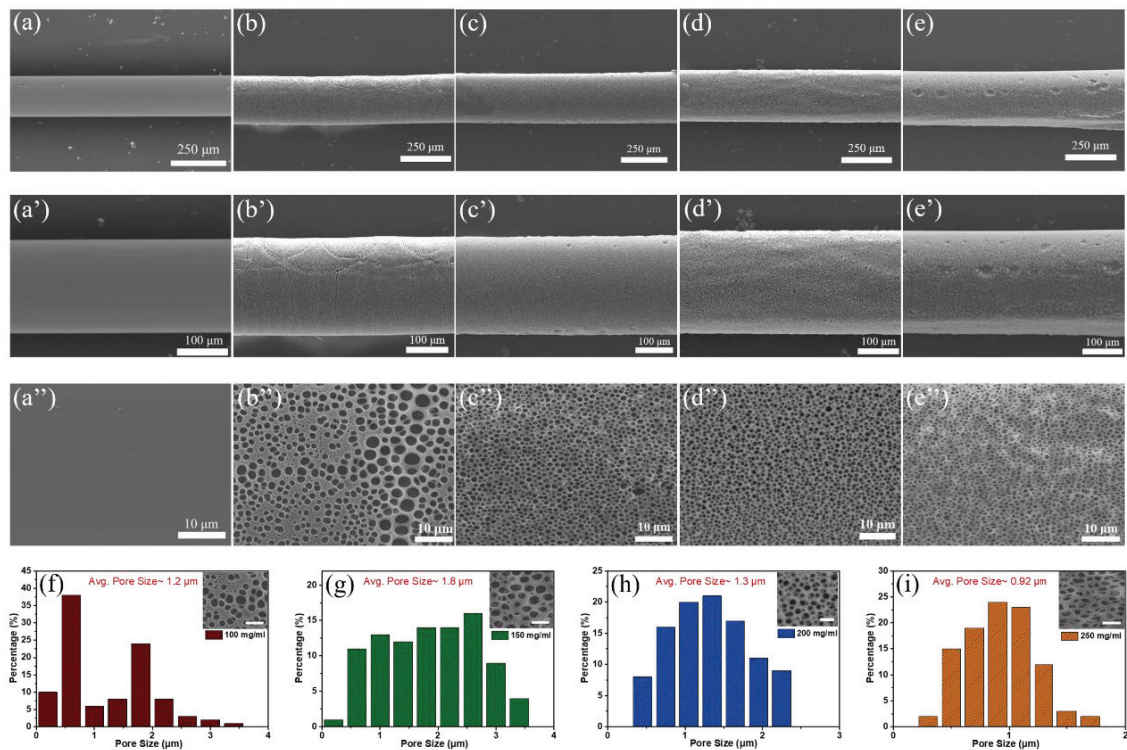


Figure 3. Typical SEM images of the pristine PET fiber (a-a''), and PET based F@HPMs prepared from SBS/CHCl₃ as polymer solution with different concentrations *via* 1D-cBF approach: (b-b'') 100 mg/ml, (c-c'') 150 mg/ml, (d-d'') 200 mg/ml, (e-e'') 250 mg/ml, and (f-i) their pore size distributions. Scale bar of (f-i): 5 μm

From the above results, an appropriate solvent and solution concentration are key factors in forming regular and uniform HPMs during the 1D-cBF process. Solvents that have different water solubility, vapor pressure, and interfacial tension with water can significantly change the shape of porous microstructure as well as the spacing distance between these porous structures. Besides, a polymer solution with insufficient concentration cannot uniformly cover the whole surface of a fiber, resulting in an irregular surface microstructure, while an excessive concentration of the solution would introduce some surface defects on the obtained F@HPMs due to its high viscosity. The optimal solution concentration in the 1D-cBF process to form

ideal F@HPMs is between 150-200 mg/ml. Furthermore, the concentration would also affect the pore size and regularity of the HPMS, which implies that the F@HPMs with adjustable and controllable surface microstructures can be achieved by adjusting these experiment parameters mentioned above.

3.3. Influence of Brick Materials and Fiber Substrates on the Formation of F@HPMs

The characteristic of polymer brick materials used in 1D-cBF process also plays an important role in the formation of F@HPMs. The brick materials can be roughly divided into two categories: amphiphilic and nonamphiphilic.²⁸ The brick material used in the above experiments was SBS, a typical multiblock copolymer with the characteristic of nonamphiphilic. During the 1D-cBF process, SBS was precipitated around the water nuclei with the evaporation of solution, followed by forming a layer to stabilize the water droplets and gradually evolved into HPMS.⁴³ PMMA is a hydrophobic linear homopolymer that could also be used as brick material, as shown in Figure 4a-c. The PET-based F@HPMs prepared from PMMA/CHCl₃ with a concentration of 150 mg/ml *via* 1D-cBF approach showed a similar surface porous microstructure as F@HPMs prepared from SBS/CHCl₃ under the same condition. PDMS-g-PAs, however, is an amphiphilic polymer composed of the hydrophobic linear backbone of PDMS and hydrophilic segments of polyacrylic acid and polymethacrylic acid. The PET-based F@HPMs prepared from PDMS-g-PAs/CHCl₃ with a concentration of 150 mg/ml *via* 1D-cBF approach are shown in Figure 4d-f. It can be found that the pore size of HPMS is quite large,

approximately 55 μm . Besides, the pore shape formed on the fiber surface is also different from those by SBS/ CHCl_3 at the same conditions, due to their diverse mechanism of water stabilization. The PDMS-g-PAs can stabilize water droplets by assembling the amphiphilic molecules at the water/solution interface to form a protective layer. After the complete evaporation of solution and water droplets, many small holes with the size ranging from 0.5-1.2 μm were left inside of each HPM unit (see Figure 3f). The hole size is smaller than those of HPMS by 2 orders of magnitude, thereby forming a kind of novel hierarchical HPMS on the fiber surface.

To further demonstrate the feasibility of this novel 1D-cBF strategy on different 1D continuous substrates, a silver-plated polyester (SPP) multifilament fiber, as well as a steel multifilament fiber composed of loose and long fibers with complex structures (insets of Figure 4g and 4j) were also used to replace the PET single fiber, respectively. After fabricating by the same 1D-cBF approach with SBS/ CHCl_3 as polymer solution and at the concentration of 150 mg/ml, similar HPMS with identical multifilament fiber profiles were observed, as demonstrated in Figure 4g-i and Figure 4j-l, respectively. Magnified views of these two resultant F@HPMS show the most significant advantages of this 1D-cBF technique: this strategy can directly construct intact and continuous HPMS even at the sharply curved surface (see arrows in Figure 4i and 4l). It is noteworthy that directly assembling materials with unique microstructures at the loose and uneven surface of 1D substrates meanwhile maintain their unique surface profiles is quite difficult and challenging by the conventional techniques. These results confirm that in addition to the single fiber with a smooth surface, the 1D-cBF strategy can also be applied to

other 1D continuous substrates with complex structures and uneven surface morphologies.

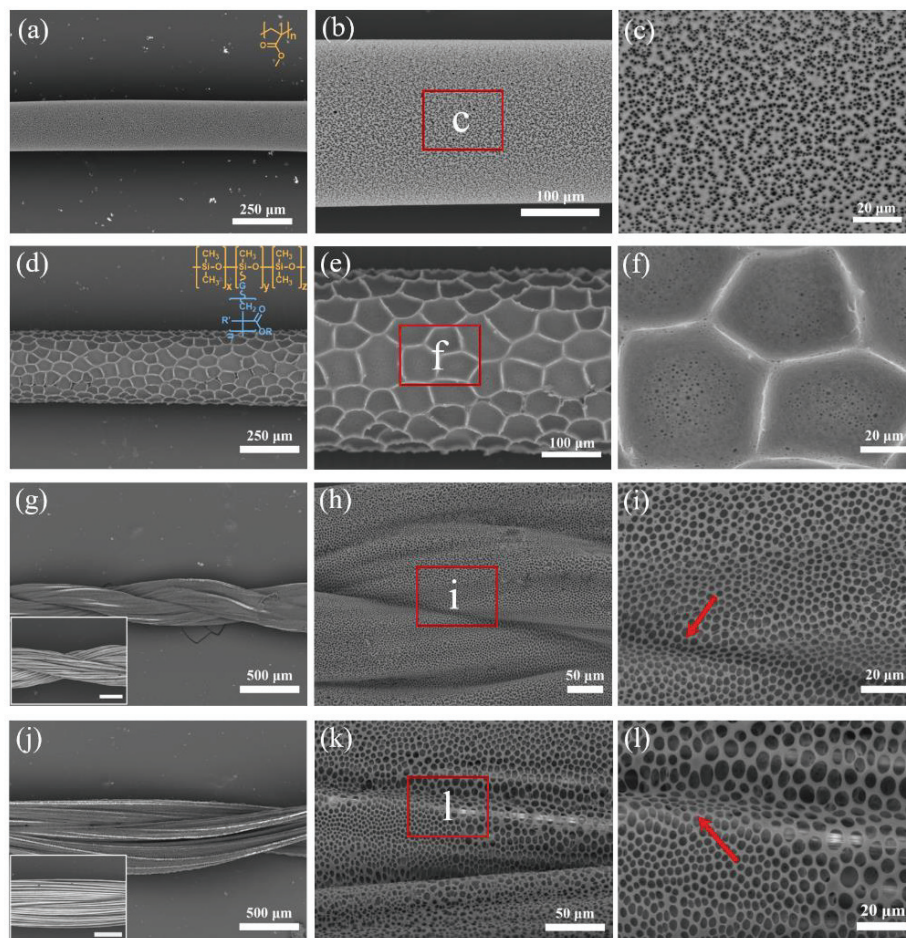


Figure 4. Typical SEM images of F@HPMs using different polymer bricks and substrates with the solution concentration of 150 mg/ml *via* 1D-cBF approach: (a-c) the PET-based F@HPMs prepared from PMMA/CHCl₃, the inset of (a) is the chemical structure of PMMA, (d-f) the PET-based F@HPMs prepared from PDMS-*g*-PAs/CHCl₃, the inset of (d) is the chemical structure of PDMS-*g*-PAs, where G = graft, R' = H or CH₃, R is a mixture of H, C₁ to C₄ esters, (g-i) the SPP-based F@HPMs prepared from SBS/CHCl₃, the inset of (g) is a pristine SPP multifilament fiber, and (j-l) the steel-based F@HPMs prepared from SBS/CHCl₃, the inset of (j) is a pristine steel multifilament fibers. Scale bar of the insets of (g) and (j): 200 μm.

3.4. Incorporation of HF@HPMs with Functional Nanomaterials

Benefiting from their larger specific surface area, porous structures were considered as great platforms for loading various functional components. Nevertheless, porous structures themselves cannot help to form a homogenous distribution of nanomaterials on the fiber surface. A detailed survey of the literature shows that the major difficulty in combining functional nano-additives with 1D continuous fibers lies in the aggregate tendency of the nanomaterials, which would inevitably affect their service efficiency and result in unnecessary waste.^{44,45} Another encouraging advantage of the 1D-cBF approach is that various nanomaterials can be straightforwardly loaded on the porous microstructures of F@HPMs by a simple one-step fabrication method. More importantly, the loaded nanomaterials show an alleviate embedded phenomenon, making the 1D-cBF approach an ideal method to fabricate HF@HPMs with customized functionalities. As illustrated in Figure 5a Route I, when using a conventional coating method to incorporate nanocomponents on the 1D fiber surface, no porous structure can be formed on the fiber surface, and the nanocomponents tend to aggregate with each other. After the evaporation of the solvent, almost all nano-additives are embedded in the solid coating layer. On the contrary, when conducting the incorporation process *via* 1D-cBF approach, the nanocomponents are self-assembling at the water droplet-solution interface owing to the synergistic effect of 1D-cBF process and the Pickering emulsion effect,^{46,47} as illustrated in Figure 5a Route II. The obtained HF@HPMs show conformal porous microstructures on its surface, and nanocomponents can well disperse in these porous platforms with an alleviative embedded phenomenon and enlarged exposing areas. Figure 5b-d shows a typical hybrid SPP multifilament fiber that incorporates with TiO₂ NPs using the conventional coating method (i.e.,

TiO₂/HF@Solid coating). The surface of the obtained TiO₂/HF@Solid coating is quite smooth without any porous microstructure. And it can be seen clearly that the TiO₂ NPs are totally embedded into the solid coating (see arrows in Figure 5d). The SEM images of TiO₂/HF@HPMs prepared from 1D-cBF process (Route II) are shown in Figure 5e-h. Continuous and regular HPMs were observed on the fiber surface, and many of these pores were found to be decorated with nanoparticles by mechanical interlock. These results confirm that the 1D-cBF approach can be utilized to straightforwardly incorporate TiO₂ NPs with 1D fiber to fabricate a novel kind of HF@HPMs with homogenously distributed TiO₂ and larger exposing area for enhanced functional applications.

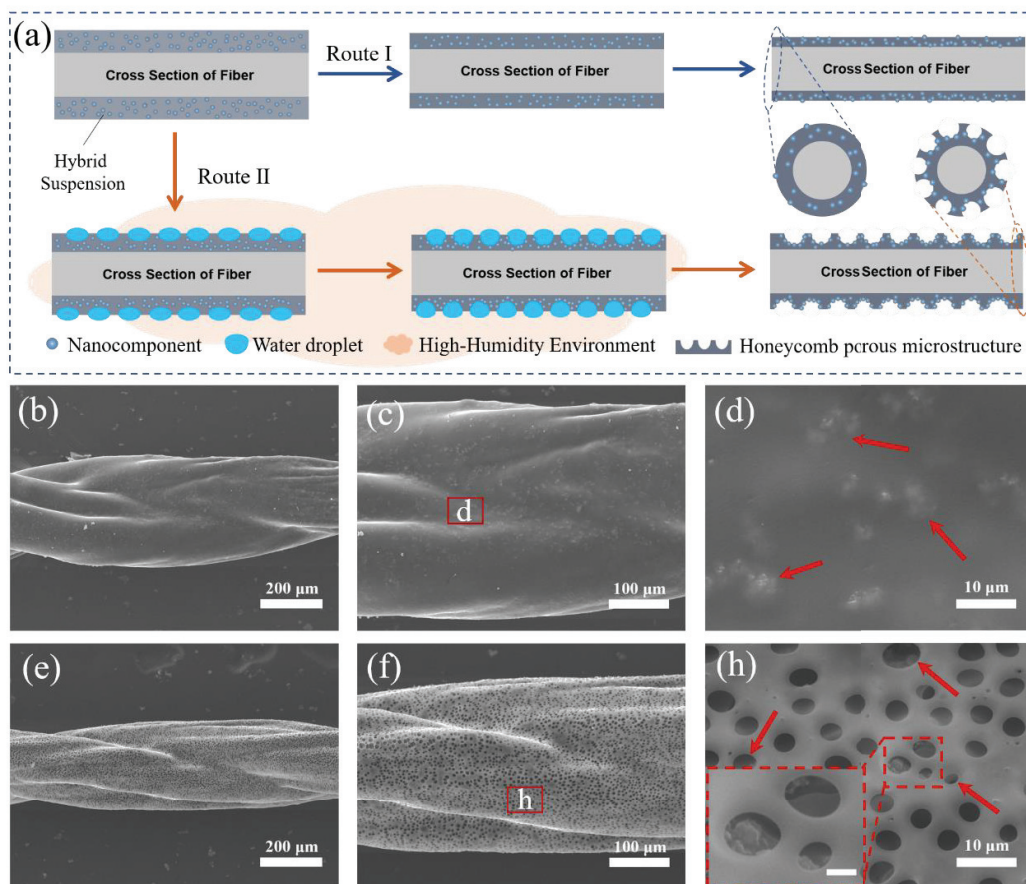


Figure 5. (a) Schematic cross-sectional diagrams of: (Route I) Nanocomponents aggregate and embed inside the solid coating layer during the conventional coating method and (Route II)

Nanocomponents self-assemble at the water droplet-solution interface during the 1D-cBF process. And SEM images of TiO₂/HF@Solid coating (b-d) and TiO₂/HF@HPMs (e-h) at different magnifications, the inset of (h) is its magnified view (scale bar: 2 μm).

To investigate the feasibility and versatility of the 1D-cBF strategy to incorporate various functional nano-additives with different kinds of fibers for the straightforward fabrication of HF@HPMs, various nanomaterials including TiO₂ NPs, Cu NPs, ZnO NWs, and Ag NWs were employed, and then further combined with SBS/CHCl₃ polymer solution to form the hybrid suspension, respectively. The additives/polymer was set at 1:20 in mass ratio. The HF@HPMs were directly prepared with these hybrid suspensions *via* the same 1D-cBF process. Figure 6a and its inset show a typical PET-based HF@HPMs incorporated with Cu NPs, and it can be seen clearly that the obtained HF@HPMs has a similar microstructure as F@HPMs without the addition of nanomaterials (see Figure 3). Besides, some particulate nanocomponents can be found inside of porous structure on the fiber surface (see arrows in Figure 6a), implying that Cu NPs are successfully loaded on the HF@HPMs. These particles are further confirmed as Cu NPs by EDS (Figure 6c). Figure 6d-e shows a PET-based HF@HPMs incorporated with TiO₂ NPs. Similarly, some pores were found to be decorated with nanoparticles, and the EDS spectrum (Figure 6f) confirmed the TiO₂ particles. The NPs normally act as stabilizers during the 1D-cBF process, and they will self-assemble onto the interface of water/solution by Pickering emulsions effect and form a protective layer around the water droplets that help the formation of HPMs. The different physicochemical properties of the NPs (e.g., size, shape and amphiphilicity) will influence this process, and therefore, the resultant morphology of porous

structures may slightly vary when incorporating with different NPs.^{48,49} In addition to the nanoparticles, some functional nanowires with a high length-diameter ratio were also used to incorporate with HF@HPMs. In contrast with NPs, the length of NWs can even exceed the average diameter of the porous structures (0.92-1.8 μm). During the 1D-cBF process, the NWs may stretch across the whole water droplets, help the growth of these water droplets and produce a larger pore size after the water are removed, as demonstrated in Figure 6g-h. The resultant porous microstructures served as frameworks to stabilize the NWs meanwhile provided a large exposing area. The EDS presented that the circled area in Figure 6h mainly includes Zn, O, and C elements, which confirms the nanowires inside pore are ZnO NWs. Moreover, the steel multifilament fibers were chosen as substrates to verify the feasibility of 1D-cBF strategy to incorporate nanomaterials with 1D continuous fibers that have complex surface morphology. As shown in Figure 6j, complex steel-based HF@HPMs incorporated with Ag NWs were successfully prepared. The corresponding EDS result of the circled area is also shown in Figure 6l. There are mainly Fe, Ag, O, and C elements, where Fe element represents the steel substrate, and Ag represents the incorporated Ag NWs. Besides, the mechanical properties of the PET fibers and SPP fibers fabricated with different conditions were investigated, as shown in Figure S2. It was found that the introduction of surface porous microstructure can slightly increase mechanical strength of the resultant PET and SPP fiber as compared with their pristine counterparts. The tensile strengths of the F@HPMs were found to increase by 2% for both PET fiber and SPP fiber. Moreover, the incorporation of TiO_2 NPs with surface porous microstructure can further enhance the tensile strength of the resultant fiber

owing to the enhanced dispersive adhesion and mechanical interaction between the NPs and polymer brick.⁵⁰⁻⁵² The SEM images of the fractured area of PET-F@HPMs (Figure S3 a-c) and PET-TiO₂/HF@HPMs (Figure S3 d-f) are also obtained. As shown in Figure S3c, for the PET-F@HPMs without TiO₂ NPs, most of the microstructures near the fracture surface were found to be cracked. However, for the PET-HF@HPMs that incorporate with TiO₂ NPs (Figure S3f), the microstructures were found to deform into elliptical shape with little cracks, indicating the good interfacial adhesion between the TiO₂ NPs and polymer brick.⁵³ These results demonstrated that this new 1D-cBF strategy has promising potential for customizable fabrication of 1D functional fiber materials to meet specific requirements of advanced functional applications.

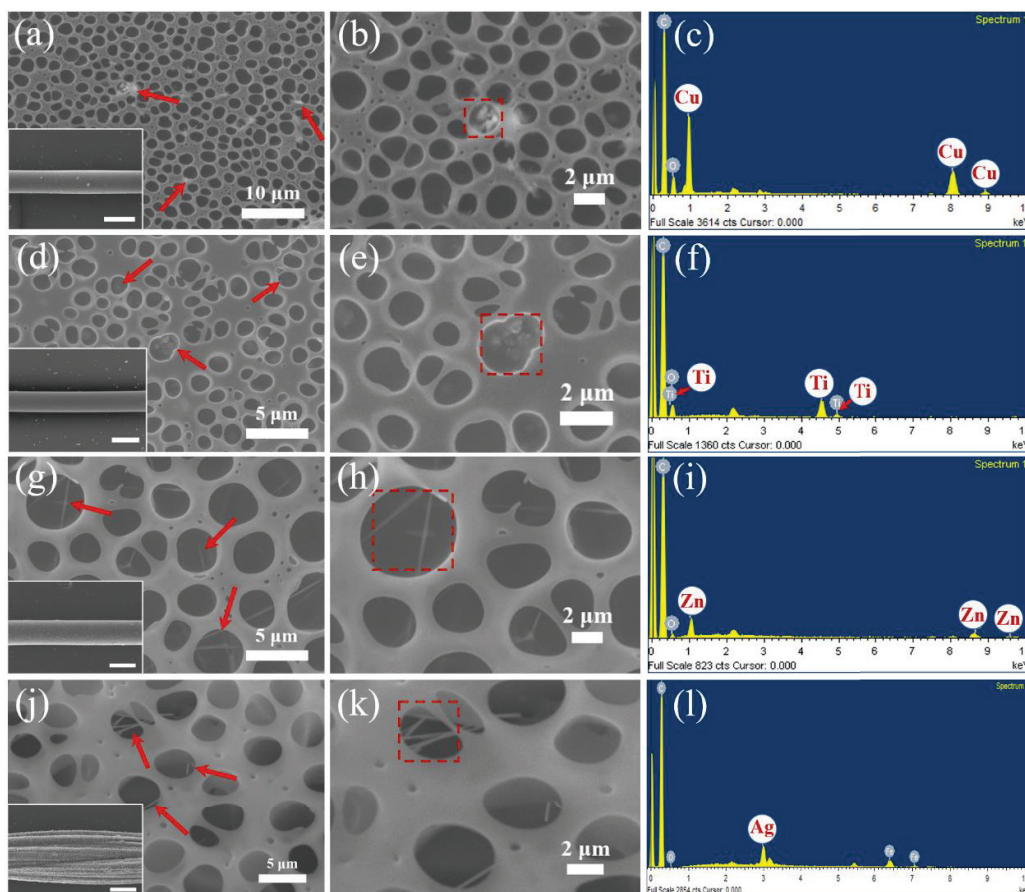


Figure 6. SEM images of HF@HPMs using SBS/CHCl₃ combined with different functional nanocomponents as hybrid solutions at the concentration of 150 mg/ml *via* 1D-cBF approach: (a, b) the PET-based HF@HPMs incorporated with Cu NPs, (d, e) the PET-based HF@HPMs incorporated with TiO₂ NPs, (g, h) the PET-based HF@HPMs incorporated with ZnO NWs, and (j, k) the complex steels-based HF@HPMs incorporated with Ag NWs. The insets are their SEM images at lower magnification correspondingly and the scale bar is 250 μm. And (c, f, i, l) are the EDS spectrums of the circled area of (b, e, h, k), respectively. Additives/polymer was set at 1:20 in mass ratio.

3.5 Photocatalytic Degradation of Organic Pollutants

As a demonstration of the feasibility of this new 1D-cBF strategy for customizable fabrication of advanced functional fibers to meet specific application requirements, a kind of functional fibers with the rational design of porous microstructures that loaded photocatalytic active

components was developed as high-performed fibers to remove organic pollutant efficiently, as shown in Figure 7. A bunch of hybrid SPP multifilament fibers incorporated with TiO₂ NPs using 1D-cBF approach (i.e., TiO₂/HF@HPMs, as shown in the left inset of Figure 7a) was chosen to conduct the photocatalytic degradation. The surface morphologies of TiO₂/HF@HPMs were shown in Figure 5e-h. Methylene blue (MB), a wide-used organic dye in textiles industries, was chosen as the model pollutant. Figure 7a shows the UV-visible absorption spectrum of MB aqueous solution (1.65×10^{-5} M) before and after photocatalytic degradation in the presence of TiO₂/HF@HPMs at different times. The aqueous solution of MB exhibits a strong absorption peak at 664 nm before the experiment, and the absorption peak was decreased significantly during the degradation process. After 25 h of UV exposure, the absorbance of MB aqueous solution was decreased by 96.5%, and the color of the solution became colorless (right inset of Figure 7a), indicating almost all MB was degraded. As contrasted with TiO₂/HF@HPMs, TiO₂/HF@Solid coating without porous microstructures (see Figure 5b-d and left inset of Figure 7b) were also chosen to evaluate their photocatalytic ability. After the same degradation process, the absorption intensity was only decreased by 65.7%, and the color of the solution was still blue (right inset of Figure 7b), indicating the incomplete degradation of MB. Furthermore, to better highlight the advantages of 1D functional fibers over the 2D fabrics, a well-tailored fabric woven from the same SPP multifilament fibers was prepared. The fabric was then modified with BF method to create surface porous microstructures that were loaded with TiO₂ (i.e., TiO₂/Fabric@HPMs, as shown in the left inset of Figure 7c). After the same UV exposure time, the absorption intensity of the MB solution

was decreased by 82.7%, and the color of the solution turned to light blue. The MB degradation efficiency of these three samples was further plotted against time, as demonstrated in Figure 7d. TiO₂/HF@HPMs shows the highest ability to remove the MB pollutant during the whole process, while the TiO₂/HF@Solid coating presents the worst performance. These results confirmed that when using the conventional coating method, most TiO₂ NPs were embedded in the solid coating (Figure 5d), resulting in the relatively low efficiency of photocatalytic degradation. With the synergistic effect of 1D-cBF technique and the Pickering emulsion effect, TiO₂ NPs can be effectively loaded on the HPMs platforms with an alleviative embedded phenomenon, which plays the most important role in the photocatalytic degradation of organic pollutant.^{54,55} Besides, benefiting from the larger specific surface area of 1D TiO₂/HF@HPMs, the contact area between photocatalytic active TiO₂ and organic pollutants also becomes larger, resulting in improved photocatalytic efficiency of TiO₂/HF@HPMs in contrast to 2D TiO₂/Fabric@HPMs. Moreover, the durability of the photocatalytic activity of TiO₂/HF@HPMs was also investigated by repeating the photodegradation process for five more times. After each process, the fibers were washed gently by DI water and then dried at 35°C in oven for 8 h. As shown in Figure 7e, the photodegradation efficiency of 1D TiO₂/HF@HPMs can maintain above 90% even after five photodegradation cycles, indicating the good durability of the prepared functional fibers.

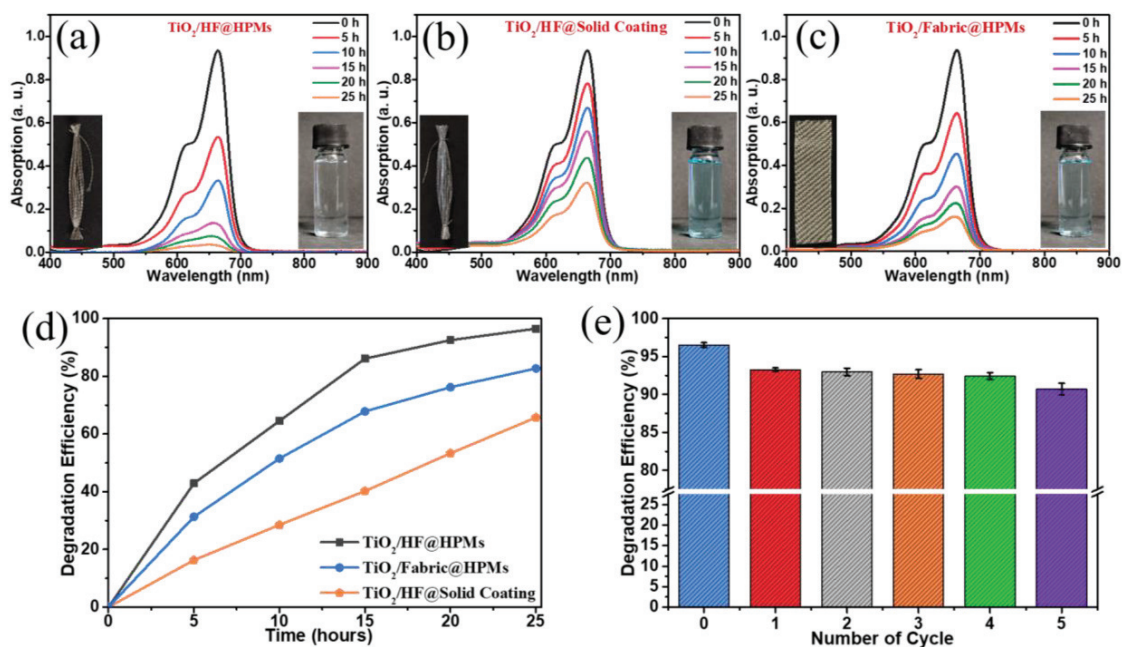


Figure 7. UV-visible absorption spectrum of methylene blue aqueous solution (1.65×10^{-5} M) before and after degradation in the presence of: (a) 1D TiO₂/HF@HPMs, (b) TiO₂/HF@Solid coating and (c) 2D TiO₂/Fabric@HPMs, insets of (a-c) are digital photographs of the corresponding fibers or fabric (left) and methylene blue aqueous solution after 25 h UV irradiation time (right). The degradation efficiency profile of different samples (d), and photocatalytic degradation efficiency of TiO₂/HF@HPMs after five cycles of testing (e).

4. Conclusions

In conclusion, a novel and facile 1D confined Breath Figure (1D-cBF) technique was developed for simple and efficient fabrication of a new kind of fibers surface-engineered with honeycomb porous microstructures (F@HPMs). The obtained F@HPMs demonstrated customizable and controllable surface microstructural morphologies by elaborately adjusting the solvent types, solution concentration, and polymer bricks. Besides, this new 1D-cBF strategy can directly construct intact and continuous HPMs on the loose and complex surface of different 1D fiber substrates meanwhile maintain their unique surface profiles. Various functional

nanocomponents can also be straightforwardly loaded on the porous microstructures of fibers by this simple one-step 1D-cBF method to form a type of hybrid F@HPMs (HF@HPMs) with customized functionalities. Moreover, benefiting from the synergistic effect of the 1D-cBF technique and the Pickering emulsion effect, the loaded nanomaterials can be well dispersed in the porous platforms with an alleviative embedded phenomenon and enlarged exposing areas. The photocatalytic degradation experiments reveal that the 1D TiO₂/HF@HPMs possess the highest efficiency (96.5%) to remove organic pollutants as compared with TiO₂/HF@Solid coating and 2D TiO₂/Fabric@HPMs. And the photodegradation efficiency can maintain above 90% even after five experimental cycles. Therefore, this 1D-cBF strategy is anticipated to extend the application fields of 1D continuous fiber materials with enhanced performance to meet a variety of specific advanced requirements.

Supporting Information

Supporting Information is available from the author.

Acknowledgment

The authors would like to acknowledge the funding support from the Research Grants Council of the Hong Kong Special Administrative Region, China (Project No. PolyU 152060/19E), for the work reported here.

References:

- (1) Granberry, R.; Eschen, K.; Holschuh, B.; Abel, J. Functionally Graded Knitted Actuators with NiTi- Based Shape Memory Alloys for Topographically Self- Fitting Wearables. *Adv. Mater. Technol.* **2019**, *4* (11), 1900548.
- (2) Dong, K.; Wang, Y.-C.; Deng, J.; Dai, Y.; Zhang, S. L.; Zou, H.; Gu, B.; Sun, B.; Wang, Z. L. A Highly Stretchable and Washable All-Yarn-Based Self-Charging Knitting Power Textile Composed of Fiber Triboelectric Nanogenerators and Supercapacitors. *ACS Nano* **2017**, *11* (9), 9490–9499.
- (3) Rein, M.; Favrod, V. D.; Hou, C.; Khudiyev, T.; Stolyarov, A.; Cox, J.; Chung, C.-C.; Chhav, C.; Ellis, M.; Joannopoulos, J. Diode Fibres for Fabric-Based Optical Communications. *Nature* **2018**, *560* (7717), 214–218.
- (4) Haines, C. S.; Lima, M. D.; Li, N.; Spinks, G. M.; Foroughi, J.; Madden, J. D. W.; Kim, S. H.; Fang, S.; De Andrade, M. J.; Göktepe, F. Artificial Muscles from Fishing Line and Sewing Thread. *Science* (80-.). **2014**, *343* (6173), 868–872.
- (5) Zhao, F.; Zhao, Y.; Cheng, H.; Qu, L. A Graphene Fibriform Resporor for Sensing Heat, Humidity, and Mechanical Changes. *Angew. Chemie* **2015**, *127* (49), 15164–15168.
- (6) Zhang, Z.; Guo, K.; Li, Y.; Li, X.; Guan, G.; Li, H.; Luo, Y.; Zhao, F.; Zhang, Q.; Wei, B. A Colour-Tunable, Weavable Fibre-Shaped Polymer Light-Emitting Electrochemical Cell. *Nat. Photonics* **2015**, *9* (4), 233–238.
- (7) Dong, K.; Peng, X.; Wang, Z. L. Fiber/Fabric-Based Piezoelectric and Triboelectric

Nanogenerators for Flexible/Stretchable and Wearable Electronics and Artificial Intelligence. *Adv. Mater.* **2020**, *32* (5), 1902549.

<https://doi.org/https://doi.org/10.1002/adma.201902549>.

- (8) Feng, C.; Huang, X. Polymer Brushes: Efficient Synthesis and Applications. *Acc. Chem. Res.* **2018**, *51* (9), 2314–2323.
- (9) Cao, R.; Wang, J.; Zhao, S.; Yang, W.; Yuan, Z.; Yin, Y.; Du, X.; Li, N.-W.; Zhang, X.; Li, X. Self-Powered Nanofiber-Based Screen-Print Triboelectric Sensors for Respiratory Monitoring. *Nano Res.* **2018**, *11* (7), 3771–3779.
- (10) Zhu, M.; Shi, Q.; He, T.; Yi, Z.; Ma, Y.; Yang, B.; Chen, T.; Lee, C. Self-Powered and Self-Functional Cotton Sock Using Piezoelectric and Triboelectric Hybrid Mechanism for Healthcare and Sports Monitoring. *ACS Nano* **2019**, *13* (2), 1940–1952.
- (11) Cao, R.; Pu, X.; Du, X.; Yang, W.; Wang, J.; Guo, H.; Zhao, S.; Yuan, Z.; Zhang, C.; Li, C. Screen-Printed Washable Electronic Textiles as Self-Powered Touch/Gesture Tribo-Sensors for Intelligent Human–Machine Interaction. *ACS Nano* **2018**, *12* (6), 5190–5196.
- (12) Wen, J.; Xu, B.; Zhou, J.; Chen, Y. Novel High-Performance Asymmetric Supercapacitors Based on Nickel-Cobalt Composite and PPy for Flexible and Wearable Energy Storage. *J. Power Sources* **2018**, *402* (February), 91–98.
<https://doi.org/10.1016/j.jpowsour.2018.09.030>.
- (13) Gong, J.; Xu, B.; Tao, X. Breath Figure Micromolding Approach for Regulating the Microstructures of Polymeric Films for Triboelectric Nanogenerators. *ACS Appl.*

Mater. Interfaces **2017**, *9* (5), 4988–4997.

- (14) Korzeniewska, E.; Tomczyk, M.; Walczak, M. The Influence of Laser Modification on a Composite Substrate and the Resistance of Thin Layers Created Using the PVD Process. *Sensors* **2020**, *20* (7), 1920.
- (15) Kong, X.; Zhu, C.; Lv, J.; Zhang, J.; Feng, J. Robust Fluorine-Free Superhydrophobic Coating on Polyester Fabrics by Spraying Commercial Adhesive and Hydrophobic Fumed SiO₂ Nanoparticles. *Prog. Org. Coatings* **2020**, *138*, 105342.
- (16) Pang, S.; Gao, Y.; Choi, S. Flexible and Stretchable Microbial Fuel Cells with Modified Conductive and Hydrophilic Textile. *Biosens. Bioelectron.* **2018**, *100*, 504–511.
- (17) Chen, Y.; Xu, B.; Gong, J.; Wen, J.; Hua, T.; Kan, C. W.; Deng, J. Design of High-Performance Wearable Energy and Sensor Electronics from Fiber Materials. *ACS Appl. Mater. Interfaces* **2019**, *11* (2), 2120–2129. <https://doi.org/10.1021/acsami.8b16167>.
- (18) Wen, J.; Xu, B.; Zhou, J.; Xu, J.; Chen, Y. 3D Patternable Supercapacitors from Hierarchically Architected Porous Fiber Composites for Wearable and Waterproof Energy Storage. *Small* **2019**, *15* (25), 1–9. <https://doi.org/10.1002/sml.201901313>.
- (19) Fei, M.-E.; Xie, T.; Liu, W.; Chen, H.; Qiu, R. Surface Grafting of Bamboo Fibers with 1, 2-Epoxy-4-Vinylcyclohexane for Reinforcing Unsaturated Polyester. *Cellulose* **2017**, *24* (12), 5505–5514.
- (20) Chen, L.; Lu, M.; Yang, H.; Avila, J. R. S.; Shi, B.; Ren, L.; Wei, G.; Liu, X.; Yin, W. Textile Based Capacitive Sensor for Physical Rehabilitation via Surface Topological

Modification. *ACS Nano* **2020**.

- (21) Cruz, J.; Fanguero, R. Surface Modification of Natural Fibers: A Review. *Procedia Eng.* **2016**, *155*, 285–288. <https://doi.org/10.1016/j.proeng.2016.08.030>.
- (22) Guan, X.; Xu, B.; Gong, J. Hierarchically Architected Polydopamine Modified BaTiO₃@P(VDF-TrFE) Nanocomposite Fiber Mats for Flexible Piezoelectric Nanogenerators and Self-Powered Sensors. *Nano Energy* **2020**, *70* (January), 104516. <https://doi.org/10.1016/j.nanoen.2020.104516>.
- (23) Wen, J.; Xu, B.; Zhou, J. Toward Flexible and Wearable Embroidered Supercapacitors from Cobalt Phosphides-Decorated Conductive Fibers. *Nano-Micro Lett.* **2019**, *11* (1), 89.
- (24) Tao, D.; Feng, C.; Cui, Y.; Yang, X.; Manners, I.; Winnik, M. A.; Huang, X. Monodisperse Fiber-like Micelles of Controlled Length and Composition with an Oligo (p-Phenylenevinylene) Core via “Living” Crystallization-Driven Self-Assembly. *J. Am. Chem. Soc.* **2017**, *139* (21), 7136–7139.
- (25) Tao, D.; Feng, C.; Lu, Y.; Cui, Y.; Yang, X.; Manners, I.; Winnik, M. A.; Huang, X. Self-Seeding of Block Copolymers with a π -Conjugated Oligo (p-Phenylenevinylene) Segment: A Versatile Route toward Monodisperse Fiber-like Nanostructures. *Macromolecules* **2018**, *51* (5), 2065–2075.
- (26) Weng, W.; Yang, J.; Zhang, Y.; Li, Y.; Yang, S.; Zhu, L.; Zhu, M. A Route toward Smart System Integration: From Fiber Design to Device Construction. *Adv. Mater.* **2020**, *32* (5), 1902301.

- (27) Feng, C.; Yi, Z.; Jin, X.; Seraji, S. M.; Dong, Y.; Kong, L.; Salim, N. Solvent Crystallization-Induced Porous Polyurethane/Graphene Composite Foams for Pressure Sensing. *Compos. Part B Eng.* **2020**, *194*, 108065.
- (28) Zhang, A.; Bai, H.; Li, L. Breath Figure: A Nature-Inspired Preparation Method for Ordered Porous Films. *Chem. Rev.* **2015**, *115* (18), 9801–9868.
- (29) Muñoz-Bonilla, A.; Fernández-García, M.; Rodríguez-Hernández, J. Towards Hierarchically Ordered Functional Porous Polymeric Surfaces Prepared by the Breath Figures Approach. *Prog. Polym. Sci.* **2014**, *39* (3), 510–554.
<https://doi.org/10.1016/j.progpolymsci.2013.08.006>.
- (30) Zhang, Y.; Wang, C. Micropatterning of Proteins on 3D Porous Polymer Film Fabricated by Using the Breath- Figure Method. *Adv. Mater.* **2007**, *19* (7), 913–916.
- (31) Gong, J.; Xu, B.; Tao, X.; Li, L. Honeycomb Microstructured Silicon Oxycarbide Sheets from Silicon- Containing Graft Copolymer Films. *Plasma Process. Polym.* **2014**, *11* (11), 1001–1009.
- (32) Gong, J.-L.; Xu, B.-G.; Tao, X.-M. Asphalt-Assisted Assembly of Breath Figures: A Robust Templating Strategy for General Fabrication of Ordered Porous Polymer Films. *RSC Adv.* **2015**, *5* (19), 14341–14344.
- (33) Guan, X.; Gong, J.; Xu, B. Three-Dimensional Conformal Porous Microstructural Engineering of Textile Substrates with Customized Functions of Brick Materials and Inherent Advantages of Textiles. *ACS Appl. Mater. Interfaces* **2020**, *12* (15), 17967–17978.

- (34) Gong, J.; Xu, B.; Tao, X. Three-Dimensionally Conformal Porous Microstructured Fabrics via Breath Figures: A Nature-Inspired Approach for Novel Surface Modification of Textiles. *Sci. Rep.* **2017**, *7* (1), 1–9.
- (35) Liu, S.; Gong, J.; Xu, B. Three-Dimensionally Conformal Porous Polymeric Microstructures of Fabrics for Electrothermal Textiles with Enhanced Thermal Management. *Polymers (Basel)*. **2018**, *10* (7), 748.
- (36) Hu, H.; Larson, R. G. Marangoni Effect Reverses Coffee-Ring Depositions. *J. Phys. Chem. B* **2006**, *110* (14), 7090–7094.
- (37) Guillen, G. R.; Pan, Y.; Li, M.; Hoek, E. M. V. Preparation and Characterization of Membranes Formed by Nonsolvent Induced Phase Separation: A Review. *Ind. Eng. Chem. Res.* **2011**, *50* (7), 3798–3817.
- (38) Servoli, E.; Ruffo, G. A.; Migliaresi, C. Interplay of Kinetics and Interfacial Interactions in Breath Figure Templating—A Phenomenological Interpretation. *Polymer (Guildf)*. **2010**, *51* (11), 2337–2344.
- (39) Wan, L.-S.; Zhu, L.-W.; Ou, Y.; Xu, Z.-K. Multiple Interfaces in Self-Assembled Breath Figures. *Chem. Commun.* **2014**, *50* (31), 4024–4039.
- (40) Wang, J.; Wang, C.-F.; Shen, H.-X.; Chen, S. Quantum-Dot-Embedded Ionomer-Derived Films with Ordered Honeycomb Structures via Breath Figures. *Chem. Commun.* **2010**, *46* (39), 7376–7378.
- (41) Gong, J.; Xu, B.; Tao, X.; Li, L. Binary Breath Figures for Straightforward and Controllable Self-Assembly of Microspherical Caps. *Phys. Chem. Chem. Phys.* **2016**,

18 (19), 13629–13637.

- (42) Wu, B.-H.; Wu, L.-W.; Gao, K.; Chen, S.-H.; Xu, Z.-K.; Wan, L.-S. Self-Assembly of Patterned Porous Films from Cyclic Polystyrenes via the Breath Figure Method. *J. Phys. Chem. C* **2018**, *122* (7), 3926–3933.
- (43) Zhu, Z.; Xu, J.; Xue, H.; Li, J. Facile Fabrication of Highly Porous Bioelectrode Membrane by Combining Breath Figure Process and Self-Assembly Process with Amphiphilic Diblock Copolymer and Hydrophilic Biocatalyst. *ACS Appl. Bio Mater.* **2018**, *1* (3), 903–909.
- (44) Green, E.; Fullwood, E.; Selden, J.; Zharov, I. Functional Membranes via Nanoparticle Self-Assembly. *Chem. Commun.* **2015**, *51* (37), 7770–7780.
<https://doi.org/10.1039/c5cc01388g>.
- (45) Xu, L.; Liang, H. W.; Yang, Y.; Yu, S. H. Stability and Reactivity: Positive and Negative Aspects for Nanoparticle Processing. *Chem. Rev.* **2018**, *118* (7), 3209–3250.
<https://doi.org/10.1021/acs.chemrev.7b00208>.
- (46) Böker, A.; Lin, Y.; Chiapperini, K.; Horowitz, R.; Thompson, M.; Carreon, V.; Xu, T.; Abetz, C.; Skaff, H.; Dinsmore, A. D.; Emrick, T.; Russell, T. P. Hierarchical Nanoparticle Assemblies Formed by Decorating Breath Figures. *Nat. Mater.* **2004**, *3* (5), 302–306. <https://doi.org/10.1038/nmat1110>.
- (47) Nie, Z.; Petukhova, A.; Kumacheva, E. Properties and Emerging Applications of Self-Assembled Structures Made from Inorganic Nanoparticles. *Nat. Nanotechnol.* **2010**, *5* (1), 15–25.

- (48) Sun, W.; Ji, J.; Shen, J. Rings of Nanoparticle-Decorated Honeycomb-Structured Polymeric Film: The Combination of Pickering Emulsions and Capillary Flow in the Breath Figures Method. *Langmuir* **2008**, *24* (20), 11338–11341.
- (49) Sun, H.; Li, H.; Bu, W.; Xu, M.; Wu, L. Self-Organized Microporous Structures Based on Surfactant-Encapsulated Polyoxometalate Complexes. *J. Phys. Chem. B* **2006**, *110* (49), 24847–24854.
- (50) Guadagno, L.; Naddeo, C.; Raimondo, M.; Barra, G.; Vertuccio, L.; Russo, S.; Lafdi, K.; Tucci, V.; Spinelli, G.; Lamberti, P. Influence of Carbon Nanoparticles/Epoxy Matrix Interaction on Mechanical, Electrical and Transport Properties of Structural Advanced Materials. *Nanotechnology* **2017**, *28* (9), 94001.
- (51) Wei, H.; Xia, J.; Zhou, W.; Zhou, L.; Hussain, G.; Li, Q.; Ostrikov, K. K. Adhesion and Cohesion of Epoxy-Based Industrial Composite Coatings. *Compos. Part B Eng.* **2020**, *193*, 108035.
- (52) Zeng, S.; Zhang, T.; Nie, M.; Fei, G.; Wang, Q. Effect of Root-like Mechanical-Interlocking Interface in Polypropylene/Aramid Fiber Composites from Experimental to Numerical Study. *Compos. Part B Eng.* **2021**, *216*, 108868.
- (53) Dang, C.-Y.; Shen, X.-J.; Nie, H.-J.; Yang, S.; Shen, J.-X.; Yang, X.-H.; Fu, S.-Y. Enhanced Interlaminar Shear Strength of Ramie Fiber/Polypropylene Composites by Optimal Combination of Graphene Oxide Size and Content. *Compos. Part B Eng.* **2019**, *168*, 488–495.
- (54) Kim, D.; Kim, H.; Chang, J. Y. Designing Internal Hierarchical Porous Networks in

Polymer Monoliths That Exhibit Rapid Removal and Photocatalytic Degradation of Aromatic Pollutants. *Small* **2020**, *16* (22), 1907555.

- (55) Lee, C.-G.; Javed, H.; Zhang, D.; Kim, J.-H.; Westerhoff, P.; Li, Q.; Alvarez, P. J. J. Porous Electrospun Fibers Embedding TiO₂ for Adsorption and Photocatalytic Degradation of Water Pollutants. *Environ. Sci. Technol.* **2018**, *52* (7), 4285–4293.